Experimental and Theoretical Studies of Rate Coefficients for the Reaction $O(^3P) + C_2H_5OH$ at High Temperatures†

Chih-Wei Wu

Department of Applied Chemistry, National Chiao Tung University, Hsinchu 30010, Taiwan

Yuan-Pern Lee*

Department of Applied Chemistry and Institute of Molecular Science, National Chiao Tung University, Hsinchu 30010, Taiwan, and Institute of Atomic and Molecular Sciences, Academia Sinica, Taipei 10617, Taiwan

Shucheng Xu

Department of Chemistry, Emory University, Atlanta, Georgia 30322

M. C. Lin

Department of Applied Chemistry and Institute of Molecular Science, National Chiao Tung University, Hsinchu 30010, Taiwan, and Department of Chemistry, Emory University, Atlanta, Georgia 30322

Received: December 28, 2006; In Final Form: March 29, 2007

Rate coefficients of the reaction $O(^3P) + C_2H_5OH$ in the temperature range 782−1410 K were determined using a diaphragmless shock tube. O atoms were generated by photolysis of SO_2 at 193 nm with an ArF excimer laser; their concentrations were monitored via atomic resonance absorption. Our data in the range 886−1410 K are new. Combined with previous measurements at low temperature, rate coefficients determined for the temperature range 297−1410 K are represented by the following equation: $k(T) = (2.89 \pm 0.09) \times 10^{-16} T^{1.62} \exp[-(1210 \pm 90)/T]$ cm^3 molecule^{-1} s^{-1}; listed errors represent one standard deviation in fitting. Theoretical calculations at the CCSD(T)/6-311+G(3df, 2p)//B3LYP/6-311+G(3df) level predict potential energies of various reaction paths. Rate coefficients are predicted with the canonical variational transition state (CVT) theory with the small curvature tunneling correction (SCT) method. Reaction paths associated with *trans* and *gauche* conformations are both identified. Predicted total rate coefficients, $1.60 \times 10^{-22} T^{3.50} \exp(16/T)$ cm^3 molecule^{-1} s^{-1} for the range 300−3000 K, agree satisfactorily with experimental observations. The branching ratios of three accessible reaction channels forming $CH_3CHOH + OH$ (1a), $CH_2CH_2OH + OH$ (1b), and $CH_3CH_2O + OH$ (1c) are predicted to vary distinctively with temperature. Below 500 K, reaction 1a is the predominant path; the branching ratios of reactions 1b,c become ∼40% and ∼11%, respectively, at 2000 K.

Introduction

Ethanol (C_2H_5OH) is an important and versatile renewable energy source; it may be used as a neat fuel, as an oxygenate additive, as a fuel extender in an internal engine via combustion,[1] or in a fuel cell via catalytic electrolytic reactions.[2] Combustion of ethanol fuel might lead to formation of toxic acetaldehyde (CH_3CHO); hence detailed modeling of the oxidation processes of ethanol is important. In addition to pyrolysis of C_2H_5OH, the reaction

$$O(^3P) + C_2H_5OH \rightarrow \text{products} \qquad (1)$$

is one of the most important processes in combustion of C_2H_5-OH. Rate coefficients of reaction 1 have been determined in the temperature range 297−886 K by several groups.[3−9] Experimental conditions, reported rate coefficients near room temperature, and Arrhenius parameters of these studies are listed in Table 1 for comparison; the corresponding Arrhenius plots are also shown in Figure 1. Grotheer et al. (designated GNK in Figure 1) employed both discharge-flow and flash photolysis methods to investigate reaction 1 and reported the only measurement of rate coefficient for $T > 450$ K; rate coefficients in the range 297−886 K may be fitted with the equation

$$k_1 = 9.88 \times 10^{-19} T^{2.46} \exp[-(932/T)] \text{ cm}^3 \text{ molecule}^{-1} \text{ s}^{-1} \qquad (2)$$

The recommended value in a literature review by Herron employed this expression.[10] Owens and Roscoe employed discharge-flow technique coupled with either chemiluminescence or mass spectrometry detection to determine k_1 in the temperature range 301−439 K and reported[6]

$$k_1 = (6.95 \pm 0.85) \times 10^{-13} \exp[-(758 \pm 204)/T)] \text{ cm}^3 \text{ molecule}^{-1} \text{ s}^{-1} \qquad (3)$$

In a later report, after considering effects from regeneration of ethanol from disproportionation reaction of the α-alkanol

† Part of the special issue "M. C. Lin Festschrift".

* To whom correspondence should be addressed. E-mail: yplee@mail.nctu.edu.tw.

10.1021/jp068977z CCC: $37.00
Published on Web 05/12/2007

TABLE 1: Summary of Reported Experimental Rate Coefficients Using Various Methods

temp/K	pressure (gas)/Torr	$10^{13}k$(~298 K)[a]	$10^{13}A$[a]	(E_a/R)/K	method[b]	ref
298	532−565 (N_2O), 10.5−50.5 (C_2H_5OH)	1.03			SP/GC	Kato and Cvetanovic (KC)[3]
301−439	1.15−1.35 (no O_2), 1.28−1.36 (excess O_2)	0.88	11.2 ± 1.3	758 ± 204	DF/CL&MS	Ayub and Roscoe (AR)[7]
298	3.70 (NO)	1.70 ± 0.30			DF/MS	Washida[8]
298−886	1.75−2.55 (N_2, NO)	0.52	c	c	DF/RF	Grotheer et al. (GNK)[9]
	5.5−220.4 (O_2, NO)				FP/RF	Grotheer et al. (GNK)[9]
782−1410	613−2039 (Ne)		1340 ± 110[d]	3040 ± 80[d]	ST/ABS	this work

[a] In units of cm^3 molecule^{-1} s^{-1}. [b] Key: SP, sensitized photolysis; GC, gas chromatography; DF, discharge flow; CL, chemiluminescence; MS, mass spectrometry; FP, flash photolysis; RF, resonance fluorescence; ST, shock tube; ABS, absorption. [c] $k(T) = 9.88 \times 10^{-19}T^{2.46}$ exp[−932/T] cm^3 molecule^{-1} s^{-1}. [d] $k(T) = (2.89 \pm 0.09) \times 10^{-16}T^{1.62}$ exp [−(1210 ± 90)/T] cm^3 molecule^{-1} s^{-1} from combined data of this work and Grotheer et al.

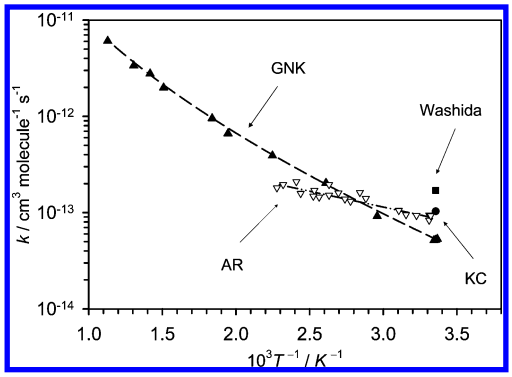

Figure 1. Arrhenius plots of previously reported k_1 for the reaction O + C_2H_5OH: GNK (▲);[9] AR(▽);[7] KC (●);[3] Washida (■).[8] Fitted results are also shown as lines of various types drawn for the temperature range of study. A combination of first character of each author's last name is used to indicate previous reports, as listed in Table 1.

radicals, Ayub and Roscoe revised this rate coefficient to become 1.6 times that listed in eq 3,

$$k_1 = (1.12 \pm 0.13) \times 10^{-12} \exp[-(758 \pm 204)/T)] \text{ cm}^3 \text{ molecule}^{-1} \text{ s}^{-1} \quad (4)$$

as shown in Figure 1 and designated as AR.[7]

Rate coefficients of this reaction show a non-Arrhenius behavior, as prersented in Figure 1 and indicated by eq 2. The rate coefficient is predicted to increase more rapidly at temperatures above 500 K, yielding an upward curved Arrhenius plot. However, even in the low-temperature range 301−439 K, rate coefficient described by eqs 4 and 2 vary by as much as 47% with activation energies varied from $E/R = 758 \pm 204$ to 1800 ± 60 K.[6,9] Experimental data for temperatures above 886 K, critical to combustion, are lacking.

There are three energetically accessible channels for this reaction at high temperature, as the oxygen atom may attack hydrogen atoms at three distinct positions,

$$O(^3P) + C_2H_5OH \rightarrow OH + CH_3CHOH \quad (1a)$$

$$\rightarrow OH + CH_2CH_2OH \quad (1b)$$

$$\rightarrow OH + CH_3CH_2O \quad (1c)$$

The branching between these channels plays important roles in the formation of the end products, inhibition of flames, formation of soot, and pollution control.[11,12] Washida used photoionization spectrometry to show that reaction 1a account for 98−100% of the total rate of reaction 1 at 300 K.[8] Dutton and co-workers employed laser-induced fluorescence under crossed molecular beam conditions to determine the branching ratio for the reaction of O + C_2H_5OD; they found that reaction 1c is faster than reactions 1a,b at a translational temperature of 3500 K.[13] Marinov compared existing experimental data with branching ratios of reactions of oxygen atoms with methane and propane to predict the temperature dependence of the rate coefficients to be[12]

$$k_{1a} = 3.12 \times 10^{-17}T^{1.85} \exp[-(918/T)] \text{ cm}^3 \text{ molecule}^{-1} \text{ s}^{-1} \quad (5)$$

$$k_{1b} = 1.56 \times 10^{-16}T^{1.70} \exp[-(2747/T)] \text{ cm}^3 \text{ molecule}^{-1} \text{ s}^{-1} \quad (6)$$

$$k_{1c} = 2.62 \times 10^{-17}T^{2.00} \exp[-(2239/T)] \text{ cm}^3 \text{ molecule}^{-1} \text{ s}^{-1} \quad (7)$$

According to this model, reaction 1c becomes increasingly important at higher temperatures and reaches a branching ratio similar to that of reaction 1a near 1400 K. By comparison with our previous investigations of the reaction O + CH_3OH,[14] the branching ratio of reaction 1c seems to be greater than expected, especially at low temperatures. To the best of our knowledge, no theoretical investigation on the O + C_2H_5OH system with high-level quantum-chemical calculations has been reported.

Because of the importance of this reaction in combustion, kinetic data at higher temperatures are needed. We have determined rate coefficients of the title reaction up to 1410 K with a diaphragmless shock tube. We also performed theoretical calculations on this reaction to compare with our experimental measurements and to understand the branching among these three H-abstraction channels at varied temperatures.

Experiments

All experiments were carried out at NCTU. The diaphragmless shock tube apparatus and technique have been described previously.[15,16] The shock tube (length 5.9 m and i.d. 7.6 cm) is coupled with a detection arrangement using atomic resonance absorption. A microwave-discharged lamp with a flowing gas mixture of ~1% O_2 in He served as a light source for spectral absorption of O atoms. Emission at 130.23, 130.49, and 130.60 nm, corresponding to transitions of $O(^3S-{}^3P_{2,1,0})$, passes perpendicularly through the shock tube near the end before entering into a vacuum UV monochromator (reciprocal linear dispersion 4.0 nm mm^{-1}, slit width 350 μm) before being detected with a solar-blind photomultiplier tube. The speed of the shock wave was determined with four pressure sensors connected to three time-frequency counters for measurements of intervals of arrival signals.

For kinetic measurements, O atoms were generated from SO_2 by laser photolysis at 193 nm. At 193 nm, the absorption cross section of SO_2 is 3.4×10^{-18} cm^2 at 1100 K and 2.8×10^{-18} cm^2 at 2000 K.[17] Light from the ArF excimer laser at 193 nm enters the shock tube from the quartz end-plate and passes along

the tube. A pulse generator was employed to trigger the photolysis laser about 50−150 μs after the arrival of the incident shock wave detected with the pressure sensor located closest to the end-plate.

Before each experiment, the system was pumped below 5.0 × 10^{-7} Torr. The temperature (T_5), density (ρ_5), and pressure (P_5) in the reflected shock regime were calculated from measured velocity of the incident shock and the initial pressure, temperature, and composition of the test gas using the ideal shock-wave theory[18] with Mirels' boundary layer corrections.[19,20] Because we are interested in the temperature range 780−1400 K, we employed Ne instead of Ar as the buffer gas.

We calibrated the concentration of O atoms in the shock tube with pyrolysis of N_2O by assuming a 100% yield of O atoms.[21] The concentration of O atoms is fitted with the equation

$$[\mathrm{O}]/10^{13}\ \text{molecule cm}^{-3} = 4.499A - 3.208A^2 + 4.356A^3 \quad (8)$$

in which absorbance $A = \ln(I_0/I)$ is calculated with the light intensity before and after production of O atoms, denoted as I_0 and I, respectively.

He (99.9995%, AGA Specialty Gases), Ne (99.999%, AGA Specialty Gases), N_2O (99.999%, Scott Specialty Gases), O_2 (99.995%, Scott Specialty Gases), and SO_2 (99.98%, Matheson) were used without further purification. C_2H_5OH (99.8%, Mallinckrodt, Analytical Reagent grade) was purified by passing the vapor through P_2O_5 to remove trace water impurity. Mixtures of C_2H_5OH in Ne (40−442 ppm) and SO_2 in Ne (192−699 ppm) were used. The concentration of C_2H_5OH in Ne was carefully calibrated with IR absorption in a multipass absorption cell.

Computational Methods

The geometries of reactants, intermediates, transition states, and products, including *gauche*- and *trans*-conformers, of the O + C_2H_5OH system were optimized at the B3LYP/6-311+G-(3df) level of theory. Single-point energies of all species were calculated with the CCSD(T)/6-311+G(3df, 2p) method,[22] based on the optimized geometries.

Rate coefficients for different reaction paths in the temperature range of T = 300−3000 K were calculated with canonical variational transition state theory (CVT) with zero curvature tunneling corrections (ZCT) and small curvature tunneling corrections (SCT) using the POLYRATE program of Truhlar et al.[23]

All calculations were carried out with Gaussian 03[24] programs using a PC cluster and the computers at the Emerson Computation Center of Emory University.

Results and Discussion

Thermal decomposition of C_2H_5OH at high temperature should be considered before characterizing the title reaction. The decomposition of C_2H_5OH not only decreases its concentration but also triggers a series of secondary reactions involving either O atoms or other reactive intermediates. Despite extensive experimental investigations of thermal decomposition of C_2H_5-OH, the branching of each channel remains uncertain.[25] We rely on theoretical predictions of the branching ratio of pyrolysis in the modeling.[26−30] According to the prediction, below 10 atm and in the temperature range 700−2500 K, the dominant channel is the formation of C_2H_4 and H_2O; at the high-pressure limit and T > 1500 K, formation of CH_3 + CH_2OH becomes dominant and the channel to form CH_3CH_2 + OH also becomes competitive. All experiments were carried out at T < 1450 K to minimize complications due to thermal decomposition of C_2H_5OH.

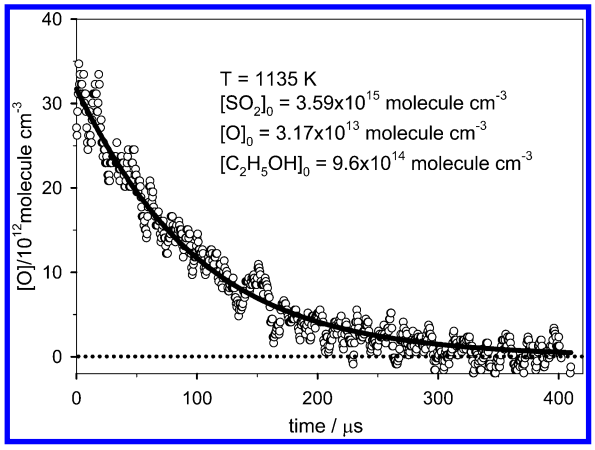

Figure 2. A typical temporal profile of [O] observed after irradiation of a sample containing SO_2 (300 ppm) and C_2H_5OH (80 ppm) in Ar. T = 1135 K, and total density = 1.20 × 10^{19} molecule cm^{-3}. The thick solid line represents fitted results using the model described in text.

A. Rate Coefficient k_1 for O + C_2H_5OH. Experiments were carried out under pseudo-first-order conditions with $[C_2H_5OH]_0 \gg [O]$. Figure 2 shows a typical temporal profile recorded for the mixture containing SO_2, C_2H_5OH, and Ne after laser photolysis at 193 nm. The concentration of O atoms at reaction period t, $[O]_t$, is derived according to eq 8. $[O]_t$ follows an exponential decay in the initial stage. The apparent pseudo-first-order rate coefficient k^I is derived with the equation

$$\ln([\mathrm{O}]_t/[\mathrm{O}]_0) = -k^{\mathrm{I}}t + at^2 - bt^3 \quad (9)$$

in which a and b are fitting parameters to account for small deviation from the exponential decay due to secondary reactions. The apparent bimolecular rate coefficient, k_1', is thus derived from

$$k_1' = k^{\mathrm{I}}/[\mathrm{C_2H_5OH}]_0 \quad (10)$$

Comparison of k_1' with the true bimolecular rate coefficient k_1 provides information on the extent of interference due to secondary reactions.

At low temperature, previous experiments indicate that reaction 1 is dominated by channel (1a).[8] Washida used photoionization spectrometry to show that reaction 1a account for 98−100% of the total rate of reaction 1 at 300 K. However, according to Marinov,[12] as temperature increases, reaction 1c becomes more important and becomes the most important channel above 1400 K. Our theoretical calculations (discussed in section C) show that reaction 1c is unimportant under our experimental conditions and the branching ratio of reaction 1b increases from ∼0.15 at 1000 K to ∼0.28 at 1400 K. Because we are only probing the decay of [O] and cannot distinguish among channels (1a)−(1c) in our experiments, in our model we employed branching ratios calculated theoretically in this work to derive the total decay coefficient. Because of the small branching ratio for reactions 1b,c, the errors in these branching ratios do not affect much the value of total rate coefficient.

Photolysis of SO_2 at 193 nm is quite efficient in generating O atoms, thus enabling us to use smaller concentrations of SO_2. In our previous experiments with CH_3OH, no significant

TABLE 2: Reaction Models Employed to Derive Rate Coefficients of O + C_2H_5OH

no.	reacn	rate expression	ref
*1a	$O + C_2H_5OH \rightarrow OH + CH_3CHOH$	fitted	
*1b	$O + C_2H_5OH \rightarrow OH + CH_2CH_2OH$	k_{1b}/k_{1a} calcd from theory	
*1c	$O + C_2H_5OH \rightarrow OH + CH_3CH_2O$	k_{1c}/k_{1a} calcd from theory	
*2	$O + OH \rightarrow O_2 + H$	$2.3 \times 10^{-11} \exp(110 \pm 100/T)$	14
3	$O + H_2 \rightarrow OH + H$	$8.44 \times 10^{-20} T^{2.67} \exp(-3167/T)$	40
4	$OH + OH \rightarrow O + H_2O$	$5.93 \times 10^{-20} T^{2.4} \exp(1063/T)$	41
5	$H_2O_2 + H \rightarrow OH + H_2O$	$1.7 \times 10^{-11} \exp(-1800/T)$	42
6	$H_2O_2 + O \rightarrow OH + HO_2$	$1.6 \times 10^{-17} T^2 \exp(-2000/T)$	43
7	$CH_3 + CH_3 (+M) \rightarrow C_2H_6 (+M)$	$k = 1.5 \times 10^{-7} T^{-1.18} \exp(-329/T)$ $k_0 = 8.77 \times 10^{-7} T^{-7.03} \exp(-1389/T)$	14[a,b]
8	$CH_3 + H (+M) \rightarrow CH_4 (+M)$	$k = 2.31 \times 10^{-8} T^{-0.534} \exp(-270/T)$ $k_0 = 7.23 \times 10^{-15} T^{-4.76} \exp(-1227/T)$	14[a,c]
9	$CH_4 + H \rightarrow CH_3 + H_2$	$3.65 \times 10^{-20} T^3 \exp(-4401/T)$	44
10	$CH_4 + O \rightarrow CH_3 + OH$	$4.7 \times 10^{-10} \exp(-6506/T)$	45
*11	$CH_3 + O \rightarrow CH_2O + H$	$(1.41 \pm 0.17) \times 10^{-10}$	14
12	$CH_3 + OH \rightarrow CH_2 + H_2O$	$1.2 \times 10^{-11} \exp(-1400/T)$	46
13	$CH_3 + OH (+M) \rightarrow CH_3OH (+M)$	$k_\infty = 1.45 \times 10^{-10} T^{0.1}$ $k_0 = 1.59 \times 10^{-6} T^{-7.4} \exp(-315/T)$	12[a,d]
14	$CH_3OH + O \rightarrow CH_2OH + OH$	$8.80 \times 10^{-20} T^{2.61} \exp(-941/T)$	14
15	$CH_3OH + O \rightarrow CH_3O + OH$	$4.15 \times 10^{-23} T^{3.64} \exp(-974/T)$	14
16	$CH_2O + OH \rightarrow HCO + H_2O$	$6.47 \times 10^{-11} \exp(-705/T)$	14
17	$CH_2O + H \rightarrow HCO + H_2$	$3.62 \times 10^{-16} T^{1.77} \exp(-1509/T)$	14
18	$CH_2O + O \rightarrow HCO + OH$	$3.0 \times 10^{-11} \exp(-1552/T)$	14
*19	$C_2H_5OH \rightarrow CH_2OH + CH_3$	$4.46 \times 10^{66} T^{-15.18} \exp(-53930/T)$	28
20	$C_2H_5OH \rightarrow C_2H_4 + H_2O$	$2.22 \times 10^{38} T^{-7.56} \exp(-38450/T)$	28
21	$C_2H_5OH + OH \rightarrow C_2H_4OH + H_2O$	$2.89 \times 10^{-13} T^{0.27} \exp(-302/T)$	12
*22	$C_2H_5OH + OH \rightarrow CH_3CHOH + H_2O$	$4.1 \times 10^{-12} \exp(-70 \pm 200/T)$	47
23	$C_2H_5OH + OH \rightarrow CH_3CH_2O + H_2O$	$1.24 \times 10^{-12} T^{0.3} \exp(-822/T)$	12
24	$C_2H_5OH + H \rightarrow C_2H_4OH + H_2$	$3.12 \times 10^{-21} T^{3.2} \exp(-3598/T)$	29
*25	$C_2H_5OH + H \rightarrow CH_3CHOH + H_2$	$2.98 \times 10^{-19} T^{2.53} \exp(-1721/T)$	29
26	$C_2H_5OH + H \rightarrow CH_3CH_2O + H_2$	$9.22 \times 10^{-47} T^{10.6} \exp(2244/T)$	29
27	$C_2H_5OH + CH_3 \rightarrow C_2H_4OH + CH_4$	$5.48 \times 10^{-22} T^{3.3} \exp(-6185/T)$	30
28	$C_2H_5OH + CH_3 \rightarrow CH_3CHOH + CH_4$	$3.31 \times 10^{-23} T^{3.37} \exp(-3842/T)$	30
29	$C_2H_5OH + CH_3 \rightarrow CH_3CH_2O + CH_4$	$3.38 \times 10^{-24} T^{3.57} \exp(-3886/T)$	30
30	$CH_3CH_2O + M \rightarrow CH_3CHO + H + M$	$1.93 \times 10^{11} T^{-5.89} \exp(-12713/T)$	12
31	$CH_3CH_2O + M \rightarrow CH_3 + CH_2O + M$	$2.24 \times 10^{14} T^{-6.96} \exp(-11972/T)$	12
32	$CH_3CHOH + CH_3 \rightarrow C_3H_6 + H_2O$	3.32×10^{-11}	12
*33	$CH_3CHOH + O \rightarrow CH_3CHO + OH$	1.66×10^{-10}	10
34	$CH_3CHOH + H \rightarrow CH_3 + CH_2OH$	3.32×10^{-11}	48
*35	$CH_3CHOH + M \rightarrow CH_3CHO + H + M$	$1.66 \times 10^{-10} \exp(-12575/T)$	12
36	$CH_3CHO + O \rightarrow CH_3CO + OH$	$2.94 \times 10^{-6} T^{-1.9} \exp(-1496/T)$	12
37	$CH_3CHO + O \rightarrow CH_2CHO + OH$	$6.18 \times 10^{-11} T^{-0.20} \exp(-1789/T)$	12
38	$CH_3CHO + H \rightarrow CH_3CO + H_2$	$7.74 \times 10^{-11} T^{-0.35} \exp(-1503/T)$	12
39	$CH_3CHO + H \rightarrow CH_2CHO + H_2$	$3.07 \times 10^{-12} T^{0.40} \exp(-2696/T)$	12
40	$CH_2CHO \rightarrow CH_2CO + H$	$1.81 \times 10^{43} T^{-9.61} \exp(-23072/T)$	12
41	$C_2H_6 + H \rightarrow C_2H_5 + H_2$	$8.97 \times 10^{-22} T^{3.5} \exp(-2620/T)$	44
42	$C_2H_6 + O \rightarrow C_2H_5 + OH$	$4.98 \times 10^{-17} T^2 \exp(-2573/T)$	44
43	$C_2H_6 + OH \rightarrow C_2H_5 + H_2O$	$1.2 \times 10^{-17} T^2 \exp(-435/T)$	42
44	$C_2H_5 + H \rightarrow C_2H_4 + H_2$	$2.08 \times 10^{-10} \exp(-4024/T)$	49
45	$C_2H_5 + H \rightarrow CH_3 + CH_3$	6.00×10^{-11}	42
46	$C_2H_5 + H \rightarrow C_2H_6$	4.98×10^{-11}	12
47	$C_2H_5 + OH \rightarrow C_2H_4 + H_2O$	4.00×10^{-11}	43
48	$C_2H_5 + O \rightarrow CH_3 + CH_2O$	2.16×10^{-10}	10
*49	$C_2H_4 + O \rightarrow CH_3 + HCO$	$(1.35 \pm 0.24) \times 10^{-17} T^{1.88} \exp(-90/T)$	50
50	$C_2H_4 + O \rightarrow CH_2CHO + H$	$7.88 \times 10^{-18} T^{1.88} \exp(-90/T)$	50
51	$C_2H_4 + H (+M) \rightarrow C_2H_5 (+M)$	$k_\infty = 1.79 \times 10^{-12} T^{0.45} \exp(-916/T)$ $k_0 = 3.06 \times 10^{-14} T^{-5} \exp(-2237/T)$	12[a,e]
52	$O + SO \rightarrow S + O_2$	$3.0 \times 10^{-11} \exp(-6980/T)$	51
53	$O + SO + M \rightarrow SO_2 + M$	$3.3 \times 10^{-26} T^{-1.84}$	52
*54	$O + SO_2 + M \rightarrow SO_3 + M$	$4.0 \times 10^{-32} \exp(-1000 \pm 200/T)$	47
55	$O + SO_2 \rightarrow O_2 + SO_2$	$8.30 \times 10^{-12} \exp(-9800/T)$	53
56	$O + CH_2OH \rightarrow CH_2O + OH$	7.0×10^{-11}	54
57	$CH_2OH (+M) \rightarrow CH_2O + H (+M)$	$k_\infty = 2.80 \times 10^{14} T^{-0.73} \exp(-16509/T)$ $k_0 = 9.98 \times 10^{9} T^{-5.39} \exp(-18209/T)$	54[a,f]

[a] k_0 and k_∞ refer to low- and high-pressure limits, respectively. The F_c parameters in the Troe equation are listed separately. Unless otherwise noted, all species are assumed to have a third body efficiency of 1.0. [b] $F_c = (1 - 0.619) \exp[-(T/73.2)] + 0.619 \exp[-(T/1180)]$. Enhanced third body coefficient (relative to N_2): $\eta_{Ar} = 0.7$. [c] $F_c = (1 - 0.783) \exp[-(T/74)] + 0.783 \exp[-(T/2941)] + \exp[-(6964/T)]$. Enhanced third body coefficient (relative to N_2): $\eta_{Ar} = 0.7$. [d] $F_c = (1 - 0.025) \exp[-(T/1 \times 10^{-15})] + 0.025 \exp[-(T/8000)] + \exp[-(3000/T)]$. Enhanced third body coefficient: $\eta_{H_2O} = 10.0$; $\eta_{H_2} = 2.0$; $\eta_{CO_2} = 3.0$; $\eta_{CO} = 2.0$. [e] $F_c = \exp[-(T/95)] + \exp[-(200/T)]$. Enhanced third body coefficient: $\eta_{H_2O} = 5.0$; $\eta_{H_2} = 2.0$; $\eta_{CO_2} = 3.0$; $\eta_{CO} = 2.0$. [f] $F_c = (1 - 0.96) \exp[-(T/67.6)] + 0.96 \exp[-(T/1855)] + \exp[-(7543/T)]$.

TABLE 3: Experimental Conditions and Rate Coefficients k_1 for the Reaction O + C_2H_5OH[a]

P_1/Torr	P_4/Torr	M_s	T_5/K	10^{-15}[SO_2]	10^{-13}[O]	10^{-14}[C_2H_5OH]	$10^{12}k_1$	k_1'/k_1
				80 ppm C_2H_5OH + 300 ppm SO_2				
56.39	2334	2.28	1300	2.81	2.37	7.51	(13.9 ± 0.3)	0.87
78.84	2339	2.12	1135	3.59	3.17	9.60	(8.9 ± 0.1)	1.11
70.60	2348	2.18	1196	3.33	2.94	8.91	(10.9 ± 0.2)	1.11
90.66	2302	2.03	1056	3.92	3.62	10.48	(7.7 ± 0.2)	1.25
128.40	2316	1.90	934	5.05	4.59	13.48	(5.1 ± 0.1)	1.35
166.80	2327	1.80	853	6.06	6.58	16.20	(3.5 ± 0.1)	1.93
				80 ppm C_2H_5OH + 502 ppm SO_2				
178.40	2322	1.74	803	10.30	9.43	16.41	(3.1 ± 0.1)	1.78
170.00	2300	1.80	852	10.30	6.40	16.50	(3.8 ± 0.1)	1.71
173.60	2338	1.76	819	10.20	8.06	16.25	(3.4 ± 0.1)	1.94
99.50	2324	1.98	1008	6.95	5.95	11.10	(6.9 ± 0.1)	1.57
140.20	2343	7.85	894	8.87	6.94	14.18	(4.7 ± 0.1)	1.73
68.25	2369	2.18	1194	5.38	4.59	8.61	(10.7 ± 0.2)	1.26
				164 ppm C_2H_5OH + 206 ppm SO_2				
57.07	2305	2.26	1275	1.92	2.18	15.37	(11.4 ± 0.3)	1.29
79.01	2310	2.12	1137	2.47	2.59	19.71	(8.2 ± 0.2)	1.04
70.79	2324	2.18	1192	2.28	2.61	18.24	(10.2 ± 0.3)	0.82
90.98	2319	2.06	1080	2.74	3.26	21.87	(7.1 ± 0.2)	1.19
128.50	2298	1.89	924	3.42	4.38	27.34	(5.2 ± 0.1)	1.13
167.30	2306	1.80	847	4.13	4.91	33.02	(3.8 ± 0.1)	1.12
126.10	2314	1.90	936	3.40	3.73	27.12	(4.7 ± 0.1)	1.46
				81 ppm C_2H_5OH + 333 ppm SO_2				
91.80	2370	2.08	1095	4.52	7.44	10.94	(9.0 ± 0.2)	1.30
55.90	2345	2.31	1331	3.13	5.21	7.59	(15.6 ± 0.3)	1.12
55.03	2340	2.32	1341	3.10	4.98	7.50	(13.9 ± 0.2)	1.26
81.21	2340	2.12	1134	4.10	6.44	9.92	(9.1 ± 0.2)	1.31
71.05	2341	2.20	1214	3.76	6.29	9.10	(11.4 ± 0.2)	1.17
130.10	2346	1.90	934	5.66	9.63	13.72	(5.7 ± 0.1)	1.72
64.30	2327	2.24	1253	3.47	5.74	8.40	(14.5 ± 0.2)	0.99
				81 ppm C_2H_5OH + 214 ppm SO_2				
55.07	2345	2.33	1348	2.00	3.70	7.54	(13.9 ± 0.2)	1.17
92.00	2351	2.08	1095	2.91	6.09	10.97	(8.9 ± 0.1)	1.24
70.50	2350	2.21	1227	2.41	4.66	9.09	(11.5 ± 0.2)	1.19
129.50	2349	1.93	958	3.70	9.42	13.94	(6.1 ± 0.1)	1.58
81.26	2341	1.97	999	2.40	5.42	9.04	(7.0 ± 0.1)	1.48
158.00	2382	1.85	890	4.25	11.28	16.00	(4.6 ± 0.1)	1.88
				442 ppm C_2H_5OH + 192 ppm SO_2				
56.40	2340	2.20	1223	1.73	2.93	39.77	(9.0 ± 0.2)	1.10
92.96	2336	2.06	1078	2.61	4.31	60.06	(6.7 ± 0.2)	1.05
70.03	2352	2.21	1223	2.15	3.40	49.38	(8.6 ± 0.2)	1.22
144.80	2295	1.87	905	3.55	5.99	81.52	(4.7 ± 0.1)	1.46
				164 ppm C_2H_5OH + 302 ppm SO_2				
71.04	2347	2.21	1225	3.42	4.02	18.56	(10.9 ± 0.2)	1.12
55.08	2340	2.32	1339	2.81	3.78	15.22	(15.1 ± 0.4)	1.14
91.28	2369	2.09	1106	4.10	5.25	22.24	(8.1 ± 0.2)	1.41
55.46	2350	2.31	1331	2.82	3.07	15.28	(12.5 ± 0.3)	1.09
149.60	2370	1.87	908	5.76	8.12	31.25	(4.5 ± 0.1)	1.63
85.96	2370	2.11	1130	3.92	4.34	21.26	(7.5 ± 0.2)	1.14
180.50	2370	1.83	876	6.75	9.26	36.58	(3.4 ± 0.1)	1.93
				40 ppm C_2H_5OH + 206 ppm SO_2				
55.22	2350	2.32	1339	1.92	2.16	3.72	(12.4 ± 0.2)	1.40
90.51	2350	2.06	1078	2.72	2.79	5.28	(8.0 ± 0.2)	1.04
71.16	2335	2.04	1061	2.11	2.37	4.10	(7.4 ± 0.1)	1.57
67.84	2350	1.72	782	1.56	1.40	3.02	(3.2 ± 0.1)	1.88
55.23	2347	2.33	1344	1.92	1.98	3.73	(14.1 ± 0. 5)	1.22
68.83	2350	2.23	1246	2.29	2.31	4.44	(10.7 ± 0.3)	1.10
80.22	2416	2.17	1182	2.57	2.82	4.99	(10.3 ± 0.2)	1.04
				165 ppm C_2H_5OH + 504 ppm SO_2				
59.18	2351	2.29	1307	4.97	5.92	16.22	(12.5 ± 0.3)	1.30
92.45	2348	1.97	997	6.43	7.72	20.98	(7.2 ± 0.2)	1.60
71.01	2357	2.22	1232	5.74	5.78	18.74	(13.3 ± 0.6)	1.05
89.21	2375	2.10	1117	6.75	7.15	22.02	(7.6 ± 0.2)	1.33
130.00	2350	1.93	962	8.78	10.15	28.67	(5.6 ± 0.2)	1.48
58.44	2450	2.31	1331	4.96	4.78	16.20	(12.5 ± 0.3)	1.08
154.30	2358	1.86	900	9.87	9.55	32.20	(4.3 ± 0.1)	1.86
				80 ppm C_2H_5OH + 699 ppm SO_2				
58.30	2348	1.82	863	4.98	3.87	5.73	(4.3 ± 0.1)	1.53

TABLE 3: (Continued)

P_1/Torr	P_4/Torr	M_s	T_5/K	$10^{-15}[SO_2]$	$10^{-13}[O]$	$10^{-14}[C_2H_5OH]$	$10^{12}k_1$	k_1'/k_1
				80 ppm C_2H_5OH + 699 ppm SO_2				
58.61	2372	1.82	863	5.01	3.31	5.76	(3.6 ± 0.1)	1.6 8
55.37	2392	1.82	867	4.75	3.15	5.46	(4.7 ± 0.1)	1.45
58.84	2390	1.76	816	4.78	3.03	5.50	(3.8 ± 0.1)	1.83
53.06	2392	2.05	1073	5.41	4.98	6.21	(7.7 ± 0.2)	1.78
49.00	2397	2.39	1410	5.97	5.44	6.86	(19.7 ± 0.7)	1.34
51.13	2392	2.27	1287	5.90	5.31	6.77	(14.0 ± 0.5)	1.22
52.16	2392	2.36	1381	6.28	6.06	7.21	(18.7 ± 0.6)	1.55
				40 ppm C_2H_5OH + 404 ppm SO_2				
55.51	2364	2.32	1339	3.79	4.63	3.72	(15.4 ± 0.4)	1.18
90.29	2331	2.07	1085	5.36	6.13	5.27	(8.4 ± 0.2)	1.53
65.53	2335	2.22	1240	4.27	5.46	4.19	(14.0 ± 0.2)	1.42
99.56	2337	2.04	1058	5.81	7.58	5.70	(8.1 ± 0.2)	1.87
129.10	2335	1.93	964	7.00	8.16	6.88	(5.1 ± 0.1)	2.13
99.60	2335	2.03	1056	5.80	8.45	5.69	(8.4 ± 0.2)	1.83

[a] Key: P_1, pressure of reactant gas mixture; P_4, pressure of driver gas; M_s, Mach number; T_5, temperature of reaction. Concentrations are in units of molecule cm^{-3}, k_1 in cm^3 $molecule^{-1}$ s^{-1} are fitted with kinetic modeling, and k_1' are derived from pseudo-first-order decays; see text.

variations in derived rate coefficients were observed for photolysis of SO_2 at 193 and 248 nm. The absorption cross section of C_2H_5OH at 193 nm, 6.5×10^{-19} cm^2,[31] is similar to that of CH_3OH, 3.2×10^{-19} cm^2;[32] hence, the effect of photolysis of C_2H_5OH at 193 nm is small.

Several interference reactions need to be considered. According to modeling, at 1500 K and $[C_2H_5OH]_0 = 2.66 \times 10^{15}$, $[SO_2]_0 = 2.74 \times 10^{15}$, and $[Ne] = 1.33 \times 10^{19}$ molecule cm^{-3}, less than 20% of C_2H_5OH decomposes within 90 μs; they proceed via the following paths:

$$C_2H_5OH\ (+M) \rightarrow C_2H_4 + H_2O\ (+M) \qquad (11a)$$

$$\rightarrow CH_2OH + CH_3\ (+M) \qquad (11b)$$

The products CH_2OH and CH_3 react rapidly with O atoms

$$O + CH_2OH \rightarrow CH_2O + OH \qquad (12)$$

$$O + CH_3 \rightarrow CH_2O + H \qquad (13)$$

Hence, subsequent reactions involving H and OH need to be considered. Reactions of O atoms with the major product of reaction 1,

$$O + CH_3CHOH \rightarrow CH_3CHO + OH \qquad (14)$$

also needs consideration; this reaction is responsible for production of OH in addition to the title reaction.

Because we used SO_2 as the source of O atoms, reactions involving SO, SO_2, and SO_3 should also be considered:[14]

$$O + SO \rightarrow S + O_2 \qquad (15a)$$

$$O + SO\ (+M) \rightarrow SO_2\ (+M) \qquad (15b)$$

$$O + SO_2\ (+M) \rightarrow SO_3\ (+M) \qquad (16a)$$

$$O + SO_2 \rightarrow SO + O_2 \qquad (16b)$$

We modeled observed temporal profiles of [O] with a commercial kinetic modeling program FACSIMILE.[33] The reactions employed in the model are listed in Table 2; the program is basically a simplified version of that employed by Marinov[12] with additional reactions involving S and SO_x and with updated rate coefficients. The rate coefficients are obtained from listed literature unless noted. It should be noted that inclusion of 57 reactions in the model is only for completeness. If we use a further simplified model with 10 major reactions (marked with an asterisk in Table 2), the results are within 5% of those derived with a more complete model.

Because the laser was triggered about 50−150 μs after arrival of the reflected shock wave at the observation zone, pyrolysis of C_2H_5OH before generation of O atoms should be taken into account, especially at high temperature. We modeled these reactions in two separate periods: the first period started from the arrival of the reflected shock wave and ended with the arrival of the photolysis laser pulse, and the second period started on arrival of the photolysis laser pulse. In the first period, we used $[O] = 0$ to derive concentrations of all reactants and intermediates at the end of this period, which were then employed in the second period, along with experimentally observed concentration of laser-produced O atoms, to model the temporal profile of [O]. In the fitting, the branching ratio of the title reaction was calculated quantum-chemically in this work, literature values of rate coefficients of all reactions in the model except the title reaction k_1 were held constant, and the bimolecular rate coefficient k_1 was varied to yield the best fit.

Experimental conditions and values of k_1 for 71 measurements in a temperature range 782−1410 K using mixtures of various concentrations of C_2H_5OH (40−442 ppm) and SO_2 (192−699 ppm) are summarized in Table 3. Ranges of reactant concentrations are as follows: $[C_2H_5OH]_0 = (0.30-8.15) \times 10^{15}$ molecule cm^{-3}; $[SO_2]_0 = (1.56-10.3) \times 10^{15}$ molecule cm^{-3}; $[O]_0 = (1.40-11.3) \times 10^{13}$ molecule cm^{-3}; $[Ne] = (6.80-22.4) \times 10^{18}$ molecule cm^{-3}. There is no obvious systematic deviation for a specific set of data, supporting that our model is adequate. Values of k_1'/k_1, also listed in Table 3, indicate that the pseudo-first-order model in general yields rate coefficient greater by as much as 2.1 times the true value and secondary reactions should be taken into account in these cases. Typically the deviation is smaller when $[C_2H_5OH]/[O]$ and the temperature are greater.

Sensitivity analysis has been performed for representative conditions near 1100, 1200, and 1300 K; the results are shown in Table 4. The rate coefficient of the title reaction is most sensitive to variations of rate coefficients of reactions 11, 25, 33, 35, and 54 at low temperatures and reactions 11, 19, 30, 33, 35, and 54 at high temperatures. In most cases, at temperatures below 1450 K the rate coefficient k_1 varies by less than 20% if the rate coefficient of one of the above reactions was varied by a factor of 2. In the extreme case at temperatures near 1450 K at which pyrolysis of C_2H_5OH

TABLE 4: Sensitivity Factors ∂ln [*O*]/∂ln *k* of Important Reactions in the Mechanism for the System O + C_2H_5OH under Various Experimental Conditions

	top 10 important reacns									
expt conditns at ~1300 K	R11	R19	R23	R30	R31	R33	R35	R37	R49	R54
C_2H_5OH (40 ppm) + SO_2 (652 ppm)	−0.24	−0.14	−0.03	0.04	−0.04	−0.03	0.03	−0.07	−0.07	−0.14
C_2H_5OH (165 ppm) + SO_2 (504 ppm)	−0.87	−0.28	−0.19	0.28	−0.17	−0.24	0.25	−0.17	−0.16	−0.38
C_2H_5OH (164 ppm) + SO_2 (206 ppm)	−0.49	−0.19	−0.09	0.11	−0.11	−0.14	0.13	−0.07	−0.09	−0.14

	top 10 important reacns									
expt conditns at ~1200 K	R8	R11	R23	R25	R30	R31	R33	R35	R37	R54
C_2H_5OH (442 ppm) + SO_2 (192 ppm)	0.02	−0.26	−0.07	−0.17	0.08	−0.07	−0.41	0.30	−0.04	−0.04
C_2H_5OH (165 ppm) + SO_2 (504 ppm)	0.12	−0.56	−0.20	−0.08	0.20	−0.19	−0.34	0.35	−0.13	−0.45
C_2H_5OH (164 ppm) + SO_2 (206 ppm)	0.05	−0.31	−0.08	−0.10	0.12	−0.09	−0.24	0.22	−0.06	−0.18

	top 10 important reacns									
expt conditns at ~1100 K	R8	R11	R21	R23	R25	R30	R31	R33	R35	R54
C_2H_5OH (442 ppm) + SO_2 (192 ppm)	0.01	−0.16	0.04	−0.03	−0.14	0.04	−0.03	−0.49	0.23	−0.08
C_2H_5OH (165 ppm) + SO_2 (504 ppm)	0.17	−0.47	0.10	−0.10	−0.36	0.12	−0.10	−0.68	0.63	−0.58
C_2H_5OH (164 ppm) + SO_2 (206 ppm)	0.07	−0.28	0.06	−0.06	−0.23	0.07	−0.06	−0.51	0.40	−0.22

becomes more important, we found that rate coefficient k_1 would increase by as much as 15% if k_{11} were neglected in the model.

Some representative decay curves covering the whole temperature range of study were also modeled with a complete model consisting of 372 reactions employed by Marinov,[12] with updated rate coefficients for reactions 2, 3, 18, 19, 21, 25, 29, 34, 46, 47, 60, 107, 108, 110, 130, 132, 135, 137, 138, 139, 143, 144, 145, 159, 191, 193, 204, and 205 in their model, reactions involving sulfur compounds listed as reactions 15 and 16 in this paper, and two additional reactions (reactions 15 and 57 in Table 3) not included in the model of Marinov.[12] Derived rate coefficients are similar to those listed in Table 3 using our model, with deviations less than 3%.

We tested the effect of branching ratio $k_{1a}/(k_{1a} + k_{1b} + k_{1c})$ on derived total rate coefficient k_1 by using the ratios proposed by Marinov[12] and found that derived rate coefficient k_1 varied by at most 5%. We also tested the effect of thermal decomposition of C_2H_5OH before its reaction with O atoms. Thermal decomposition of C_2H_5OH has two effects: the decrease in [C_2H_5OH] and effects due to secondary reactions involving pyrolysis products CH_3 and CH_2OH. When we took out the simulation of the first period (i.e., to assume that thermal decomposition of C_2H_5OH was negligible before the photolysis laser arrived), we found that fitted rate coefficients k_1 increased by <1% for reaction temperatures below 1200 K, indicating that the small decrease in [C_2H_5OH] during the first period was negligible. In contrast, we found that k_1 increased by <5% for temperatures at 1410 K because 6% C_2H_5OH dissociated in the first period.

Calculated branching ratios of thermal decomposition of ethanol, R19 and R20 in Table 2, in the literature have large discrepancies. The rate coefficients of R19 predicted by Li et al.[34] are smaller by factors of 0.75 and 0.40 at 1400 and 1000

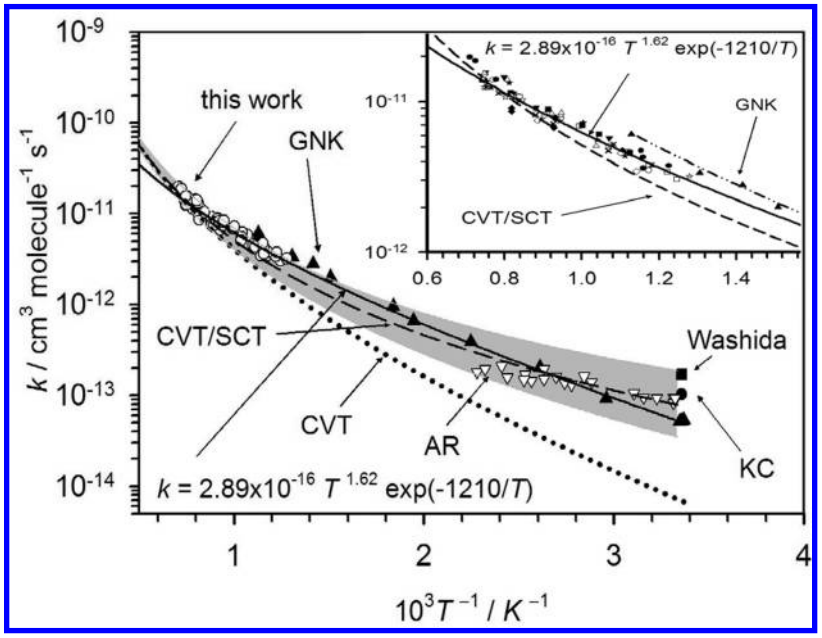

Figure 3. Comparison of experimental total rate coefficient k_1 with theoretical calculations: medium dash line, CVT with SCT tunneling correction; dotted line, CVT; ○, this work; ▲, GNK;[9] ▽, AR;[7] ●, KC;[3] ■, Washida.[8] Inset: Expanded view of data from this work. Key: ○, SO_2 (300 ppm) + C_2H_5OH (80 ppm); □, SO_2 (502 ppm) + C_2H_5OH (80 ppm); ×, SO_2 (206 ppm) + C_2H_5OH (164 ppm); ▼, SO_2 (333 ppm) + C_2H_5OH (81 ppm); ■, SO_2 (214 ppm) + C_2H_5OH (81 ppm); □, SO_2 (192 ppm) + C_2H_5OH (442 ppm); □, SO_2 (302 ppm) + C_2H_5OH (164 ppm); □, SO_2 (206 ppm) + C_2H_5OH (40 ppm); □, SO_2 (504 ppm) + C_2H_5OH (165 ppm); ●, SO_2 (699 ppm) + C_2H_5OH (80 ppm); △, SO_2 (404 ppm) + C_2H_5OH (40 ppm); ▲, GNK.[9]

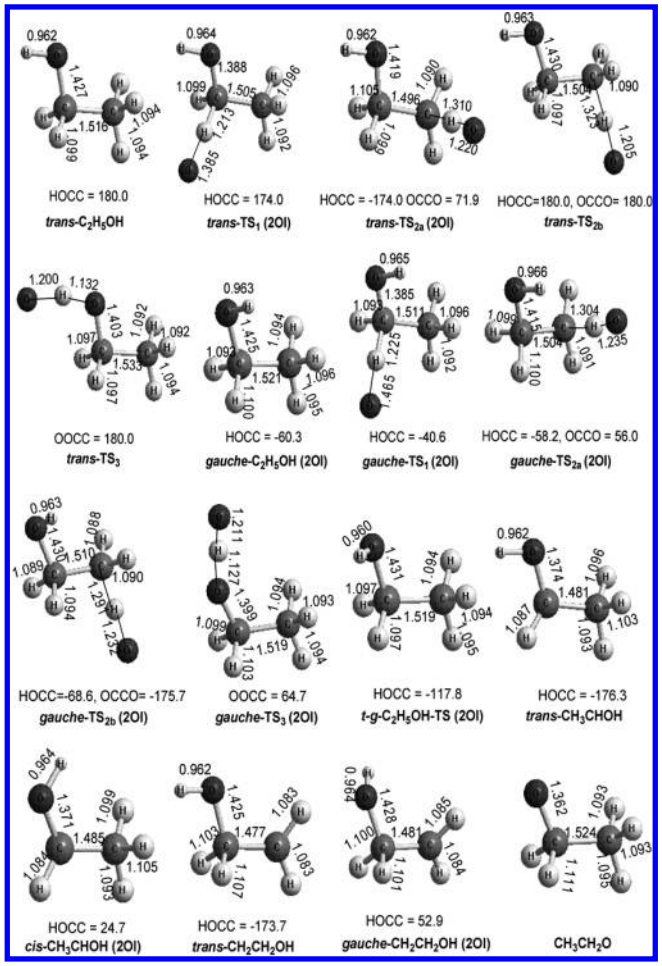

Figure 4. Geometries of reactant C_2H_5OH, transition states, and products of the O + C_2H_5OH system optimized at the B3LYP/6-311+G(3df) level. Listed bond lengths are in Å, and bond angles are in deg. 2OI indicates that two optical isomers exist for this configuration.

K, respectively, than those predicted by Park et al.[28] In contrast, rate coefficients of R20 predicted by Li et al.[34] are greater by factors of 4.8 at 1400 K and 2.9 at 1000 K than those predicted by Park et al.[28] We employed these rate coefficients reported by Li et al. in our model and derived rate coefficients of the title reaction k_1 smaller by <6% than those using the smaller values of Park et al.; the largest deviation was observed at higher temperatures and with greater concentration of SO_2.

Values of k_1 are compared with previous reports in Figure 3; an expanded view is shown in the inset. Fitting our results to an Arrhenius equation yields

$$k_1 = (1.34 \pm 0.11) \times 10^{-10} \exp[-(3040 \pm 80)/T] \text{ cm}^3 \text{ molecule}^{-1} \text{ s}^{-1} \quad (17)$$

for $782 < T/\text{K} < 1410$, in which listed errors represent one standard deviation in fitting, unless otherwise noted. Observed value of $E_a/R = 3040$ K is much greater than the value $E_a/R = 758$ K reported previously from measurements at temperatures 301−439 K,[6,7] indicating clearly the non-Arrhenius temperature dependence with an upward curvature. Our rate coefficients are smaller by 23−28% than those reported by Grotheer et al. in the overlapped range of temperature 782−886 K;[9] the deviations are within experimental error limits. Our work extends the temperature range of study from 886 to 1410 K. Fitting combined data for this work and those of Grotheer et al. yields

$$k_1 = (2.89 \pm 0.09) \times 10^{-16} T^{1.62} \exp[-(1210 \pm 90)/T] \text{ cm}^3 \text{ molecule}^{-1} \text{ s}^{-1} \quad (18)$$

B. Potential Energy Surfaces and Reaction Mechanism. As shown in Figure 4, the C_2H_5OH has *trans* (dihedral angle ϕ(HOCC) = 180.0°) and *gauche* (dihedral angle ϕ(HOCC) = 60.3°) conformers. They can transform to each other via a transition state *t-g*-C_2H_5OH-TS with a small barrier of 0.7 kcal mol^{-1}. The oxygen atom reacts with both conformers. The potential energy diagram obtained by single-point CCSD(T)/6-311+G(3df, 2p) calculations on the basis of geometries optimized at the B3LYP/6-311+G(3df) level is presented in Figure 5. Total energies of the reactants and relative energies of the transition states and products are listed in Table 5. Vibrational wavenumbers and moments of inertia of all species are summarized in Table 6.

The oxygen atom may attack C_2H_5OH at one of the two hydrogen atoms of the CH_2 group (reaction 1a), one of the three hydrogen atoms of the CH_3 group (reaction 1b), or the H atom of the hydroxyl group (reaction 1c). As shown in Figure 5, the *trans* path of reaction 1a proceeds via *trans*-TS_1 (dihedral angle ϕ(HOCC) = 174.0°) with a barrier of 4.2 kcal mol^{-1} and forms *trans*-CH_3CHOH and OH with energy −6.6 kcal mol^{-1} relative to that of the reactants. The corresponding *gauche* path has a barrier of 4.3 kcal mol^{-1} via *gauche*-TS_1 (dihedral angle ϕ-(HOCC) = −40.6°) and ΔH of −6.3 kcal mol^{-1} for formation of *cis*-CH_3CHOH.

The *trans* path for reaction 1b proceeds via the *trans*-TS_{2a} (dihedral angle ϕ(HOCC) = −174.0°, ϕ(OCCO) = 71.9°) with a barrier of 9.3 kcal mol^{-1} or the *trans*-TS_{2b} (dihedral angle ϕ(HOCC) = ϕ(OCCO) = 180.0°) with a barrier of 9.8 kcal mol^{-1} to form *trans*-CH_2CH_2OH and OH with $\Delta H = 0.7$ kcal mol^{-1}. The corresponding *gauche* path for reaction 1b proceeds via *gauche*-TS_{2a} (dihedral angle ϕ(HOCC) = −58.2°, ϕ(OCCO) = 56.0°) with a barrier of 7.7 kcal mol^{-1} or *gauche*-TS_{2b} (dihedral angle ϕ(HOCC) = 68.6°, ϕ(OCCO) = −175.7°) with a barrier of 9.7 kcal mol^{-1} to form *gauche*-CH_2CH_2OH and OH with $\Delta H = 0.3$ kcal mol^{-1}.

The *trans* path of reaction 1c proceeds via *trans*-TS_3 (dihedral angle ϕ(HOCC) = 180.0°) with a barrier of 10.7 kcal mol^{-1} and forms CH_3CH_2O and OH with $\Delta H = 2.1$ kcal mol^{-1}. The corresponding *gauche* path proceeds via *gauche*-TS_3 (dihedral angle ϕ(HOCC) = 64.7°) with a barrier of 10.0 kcal mol^{-1}.

The predicted enthalpies of reaction for the three branching reactions are compared with experimental values in Table 5. The predicted enthalpy changes for reactions 1a−c at 0 K, −6.5 ± 0.2, 0.5 ± 0.2, and 2.1 kcal mol^{-1}, are close to the experimental values −8.7 ± 0.2, 2.3 ± 0.2, and 1.7 ± 1.2 kcal mol^{-1}, respectively, on the basis of $\Delta H_{f,0}(O) = 58.99 \pm 0.02$,[35] $\Delta H_{f,0}(C_2H_5OH) = -51.88 \pm 0.12$,[35] $\Delta H_{f,0}(CH_3CHOH) = -10.5$,[36] $\Delta H_{f,0}(CH_3CH_2O) = -0.05 \pm 0.96$,[35] and $\Delta H_{f,0}(OH) = 8.87 \pm 0.07$ kcal mol^{-1};[35] $\Delta H_{f,0}(CH_2CH_2OH) = 0.57$ kcal mol^{-1} is derived from $\Delta H_{f,298}(CH_2CH_2OH) = -2.46$ kcal mol^{-1}.[37]

As shown in Figure 4, the reacting atoms O, H, and C in *trans*-TS_1 are almost linear, with ∠OHC = 177°; the length of the breaking C−H bond increases by 0.11 Å from that of *trans*-C_2H_5OH. The imaginary vibrational wavenumber of *trans*-TS_1 is 355i cm^{-1}. For *gauche*-TS_1, ∠OHC = 176° and the C−H bond length increases by 0.12 Å from that of *gauche*-C_2H_5OH. The imaginary vibrational wavenumber of *gauche*-TS_1 is 505i cm^{-1}. For *trans*-TS_{2a} and *trans*-TS_{2b}, ∠OHC = 177−8° and the C−H bond length increases by 0.22−0.23 Å from that of *trans*-C_2H_5OH; the imaginary vibrational wavenumbers are

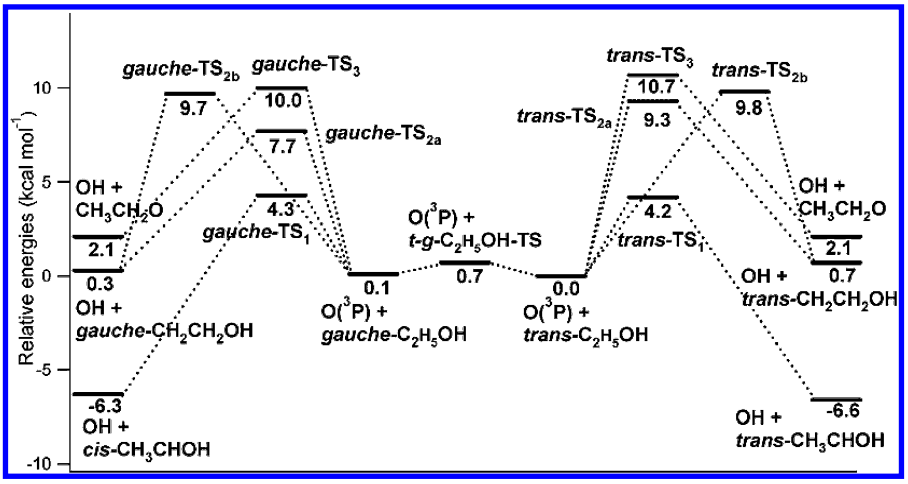

Figure 5. Potential energy diagram for various channels of the reaction O + C_2H_5OH on the basis of energies calculated with CCSD(T)/6-311+G-(3df, 2p)//B3LYP/6-311+G(3df). Listed energies are in kcal mol^{-1}.

TABLE 5: Total and Relative Energies[a] of Reactants, Transition States, and Products of the Reaction O + C_2H_5OH

species or reacns	ZPE	B3LYP/6-311+G(3df)	CCSD(T)[b]/6-311+G(3df, 2p)	ΔH_0 expt[c]
O(^{3}P) + *trans*-C_2H_5OH	0.079602	−230.105859	−229.681620	
O(^{3}P) + *gauche*-C_2H_5OH	0.0	0.1	0.1	
O(^{3}P) + *t-g*-C_2H_5OH-TS	−0.3	0.8	0.7	
trans-TS_1	−2.6	−4.8	4.2	
gauche-TS_1	−2.7	−4.3	4.7	
trans-TS_{2a}	−4.0	1.9	9.3	
gauche-TS_{2a}	−3.7	0.7	7.7	
trans-TS_{2b}	−4.1	2.9	9.8	
gauche-TS_{2b}	−3.8	2.3	9.7	
trans-TS_3	−4.7	0.1	10.7	
gauche-TS_3	−4.6	−0.5	10.0	
trans-CH_3CHOH + OH	−4.4	−11.8	−6.6	−8.7 ± 0.2
trans-CH_2CH_2OH + OH	−4.0	−3.4	0.7	2.3 ± 0.2
cis-CH_3CHOH + OH	−3.5	−11.5	−6.3	−8.7 ± 0.2
gauche -CH_2CH_2OH + OH	−3.5	−3.9	0.3	2.3 ± 0.2
CH_3CH_2O + OH	−4.6	−5.3	2.1	1.7 ± 1.2

[a] Total energies for O(^{3}P) + C_2H_5OH are in au, and relative energies for others are in kcal mol^{-1}. [b] Based on optimized geometries calculated at B3LYP/6-311+G(3df). [c] At 0 K, $\Delta H_{f,0}$ are taken from ref 35 unless noted: $\Delta H_{f,0}(O) = 58.99 \pm 0.02$ kcal mol^{-1}; $\Delta H_{f,0}(C_2H_5OH) = -51.88 \pm 0.12$ kcal mol^{-1}; $\Delta H_{f,0}(OH) = 8.87 \pm 0.07$ kcal mol^{-1}; $\Delta H_{f,0}(CH_2CH_2OH) = 0.57$ kcal mol^{-1} using $\Delta H_{f,298}(CH_2CH_2OH) = -2.46$ kcal mol^{-1};[37] $\Delta H_{f,0}(CH_3CHOH) = -10.5$ kcal mol^{-1};[36] $\Delta H_{f,0}(CH_3CH_2O) = -0.05 \pm 0.96$ kcal mol^{-1}.

TABLE 6: Vibrational Wavenumbers and Moments of Inertia I_i for the Reactants, Transition States, and Products of the Reaction O + C_2H_5OH Calculated with B3LYP/6-311+G(3df)

species	I_i (au)	vibrational wavenumbers (cm^{-1})
trans-C_2H_5OH	51.1, 193.3, 221.8	241, 285, 417, 820, 896, 1030, 1100, 1179, 1268, 1297, 1405, 1448, 1482, 1498, 1522, 2983, 3007, 3034, 3099, 3104, 3827
gauche-C_2H_5OH	52.2, 197.1, 222.9	259, 276, 420, 804, 883, 1059, 1070, 1134, 1281, 1371, 1403, 1417, 1488, 1491, 1515, 2990, 3018, 3065, 3087, 3100, 3810
t-g-C_2H_5OH-TS	51.5, 198.1, 222.9	253, 417, 800, 888, 1041, 1097, 1129, 1283, 1350, 1401, 1420, 1483, 1493, 1514, 3010, 3026, 3040, 3089, 3102, 3863, 275i
trans-TS_1	206.4, 414.5, 571.7	91, 159, 242, 377, 428, 822, 918, 968, 1056, 1152, 1179, 1199, 1278, 1398, 1407, 1438, 1477, 1488, 3010, 3030, 3095, 3120, 3808, 355i
guach-TS_1	209.8, 409.7, 565.1	127, 163, 253, 386, 448, 767, 878, 924, 1061, 1118, 1171, 1215, 1306, 1366, 1403, 1426, 1483, 1485, 3020, 3073, 3093, 3112, 3789, 505i
trans-TS_{2a}	157.2, 490.8, 584.7	80, 148, 244, 398, 486, 534, 819, 897, 1030, 1083, 1109, 1180, 1208, 1267, 1277, 1421, 1454, 1487, 2929, 3007, 3085, 3169, 3831, 1487i
gauche-TS_{2a}	182.1, 395.6, 525.2	87, 163, 382, 424, 458, 573, 821, 886, 1021, 1077, 1132, 1177, 1205, 1251, 1381, 1409, 1440, 1484, 2991, 3025, 3076, 3162, 3763, 1412i
trans-TS_{2b}	69.8, 678.8, 725.4	67, 117, 179, 360, 430, 569, 817, 891, 1013, 1047, 1155, 1173, 1179, 1247, 1295, 1429, 1472, 1518, 3004, 3034, 3087, 3169, 3812, 1504i
gauche-TS_{2b}	69.9, 689.4, 731.7	82, 116, 297, 361, 458, 557, 805, 900, 1030, 1041, 1096, 1173, 1184, 1281, 1363, 1400, 1464, 1505, 3029, 3072, 3104, 3157, 3805, 1486i
trans-TS_3	59.9, 611.7, 648.8	62, 145, 242, 253, 342, 641, 820, 889, 997, 1092, 1156, 1170, 1281, 1356, 1396, 1475, 1496, 1523, 3006, 3040, 3048, 3111, 3124, 1536i
gauche-TS_3	158.6, 414.3, 520.2	76, 160, 259, 366, 430, 615, 788, 884, 1052, 1096, 1124, 1209, 1269, 1373, 1405, 1431, 1484, 1495, 2965, 3007, 3031, 3096, 3107, 1512i
OH	0.0, 3.2, 3.2	3701
trans-CH_3CHOH	38.8, 191.3, 217.9	179, 363, 408, 540, 928, 1023, 1059, 1205, 1275, 1398, 1446, 1464, 1489, 2945, 3037, 3097, 3139, 3830
cis-CH_3CHOH	40.5, 191.1, 218.8	195, 334, 411, 564, 916, 1021, 1063, 1200, 1309, 1403, 1435, 1468, 1485, 2927, 3003, 3093, 3195, 3800
trans-CH_2CH_2OH	44.5, 180.1, 212.5	95, 269, 412, 455, 869, 957, 1058, 1108, 1216, 1266, 1420, 1459, 1484, 2891, 2944, 3158, 3267, 3829
gauche-CH_2CH_2OH	46.8, 182.9, 210.7	177, 329, 423, 537, 827, 950, 1082, 1121, 1184, 1359, 1398, 1452, 1481, 2974, 2992, 3142, 3247, 3800
CH_3CH_2O	45.1, 188.8, 211.8	46, 256, 435, 860, 886, 1070, 1097, 1239, 1327, 1389, 1408, 1485, 1493, 2882, 2893, 3031, 3096, 3106

1487i and 1504i cm^{-1}, respectively. For *gauche*-TS_{2a} and *gauche*-TS_{2b} with ∠OHC = 168 and 180°, respectively, the C−H bond length increases by 0.21 and 0.20 Å from that of *trans*-C_2H_5OH and the imaginary vibrational wavenumbers are 1412i and 1486i cm^{-1}, respectively. For *trans*-TS_3 and *gauche*-TS_3, ∠OHO = 161−162° and the C−H bond length increases by 0.17 Å from the corresponding C_2H_5OH conformer; the imaginary vibrational wavenumbers are 1536i and 1512i cm^{-1}, respectively. The geometry parameters and imaginary frequencies of the *trans* and *gauche* transition states are similar. The *trans* and *gauche* transition states can be transformed to each other by the internal rotation about the C−O single bond. The *trans* or *gauche* TS_{2a} and TS_{2b} can be transformed to each other by the internal rotation about the C−C bond.

C. Calculations and Comparison of Rate Coefficients. As shown in Figure 5, the three direct H-abstraction reaction

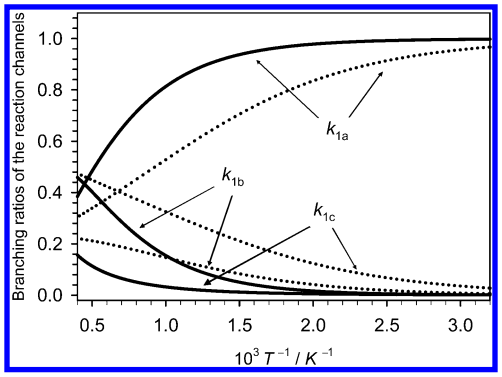

Figure 6. Branching ratios for reactions 1a−c: solid line, this work; dotted line, Marinov.[12]

channels have barriers of 4.2−10.7 kcal mol^{-1}; hence, tunneling effects for these channels should be considered. Rate coefficients for the three channels in the temperature range 300−3000 K have been computed with the CVT and the CVT/SCT methods on the basis of the geometries, vibrational frequencies, and rotational constants calculated at the B3LYP/6-311+G(3df) level and the energies calculated at the CCSD(T)/6-311+G(3df, 2p)//B3LYP/6-311+G(3df) level. Because there are two optical isomers for *trans*-TS_1, *gauche*-TS_1, *trans*-TS_{2a}, *gauche*-TS_{2a}, *gauche*-TS_{2b}, and *gauche*-TS_3, a statistical factor of 2 is employed in the calculations.

Because of the existence of the *trans*-C_2H_5OH and *gauche*-C_2H_5OH conformers and their corresponding transition states, the rate coefficient for the reaction of each conformer should be taken into account using their equilibrium concentrations at each temperature. The thermal equilibrium constant, K = [*gauche*-C_2H_5OH]/[*trans*-C_2H_5OH] = 0.87−0.97 in the temperature range 300−3000 K, can be calculated with the Chemrate Program.[38] The predicted rate coefficients for channels (1a), (1b), and (1c) are derived from rate coefficients of the *trans*-C_2H_5OH and *gauche*-C_2H_5OH reactions:[39]

$$k_{1a}(T) = (k_{trans-1a}(T) + k_{gauche-1a}(T)K)/(1+K) \quad (19)$$

$$k_{1b}(T) = (k_{trans-1b}(T) + k_{gauche-1b}(T)K)/(1+K) \quad (20)$$

$$k_{1c}(T) = (k_{trans-1b}(T) + k_{gauche-1b}(T)K)/(1+K) \quad (21)$$

In calculations of rate coefficients, the internal rotation about the C−O bond in *trans*-TS_1, TS_{2a}, and TS_{2b} have been treated as hindered rotors. Such treatments increase the total rate coefficient by 59−17% in the temperature range 300−3000 K.

To compare predicted rate coefficients with experimental data quantitatively, we fit rate coefficients predicted with CVT/SCT for channels (1a), (1b), and (1c) in the temperature range 300−3000 K to the three-parameter form to yield

$$k_{1a}(T) = 2.41 \times 10^{-19} T^{2.47} \exp(-441/T)\ \text{cm}^3\ \text{molecule}^{-1}\ \text{s}^{-1} \quad (22)$$

$$k_{1b}(T) = 1.61 \times 10^{-21} T^{3.23} \exp(-2344/T)\ \text{cm}^3\ \text{molecule}^{-1}\ \text{s}^{-1} \quad (23)$$

$$k_{1c}(T) = 2.43 \times 10^{-27} T^{4.73} \exp(-869/T)\ \text{cm}^3\ \text{molecule}^{-1}\ \text{s}^{-1} \quad (24)$$

The total rate coefficients calculated with the CVT and CVT/SCT methods for the temperature range 300−3000 K are represented as

$$k_1(T) = 3.77 \times 10^{-20} T^{2.86} \exp[-(1265/T)]\ \text{cm}^3\ \text{molecule}^{-1}\ \text{s}^{-1} \quad (25)$$

and

$$k_1(T) = 1.60 \times 10^{-22} T^{3.50} \exp(16/T)\ \text{cm}^3\ \text{molecule}^{-1}\ \text{s}^{-1} \quad (26)$$

respectively. At 300 K, rate coefficients of reactions 1a−c predicted with CVT/SCT are 10, 58, and 1330 times those predicted with CVT, respectively, resulting to a difference in total rate coefficient of about a factor of 10. The total rate coefficients calculated with CVT (dotted line) and CVT/SCT (medium dash line) are plotted in Figure 3 to compare with experimental data of GNK,[9] AR,[7] KC,[3] Washida,[8] and this work. In general, rates predicted with CVT/SCT are in satisfactory agreement with experimental values, indicating the SCT method treats tunneling effects adequately. At low temperatures, rate coefficients predicted with CVT/SCT are slightly greater than experimental values of GNK[9] but within uncertainties of other experiments. An expanded plot for high temperatures is shown in the inset of Figure 3. At high temperatures, predicted rate coefficients fit satisfactorily with experimental data of this work but slightly smaller than those of GNK.[9] The uncertainty of the barriers of transition states has significant effect on the rate coefficient at low temperatures. The uncertainty of the calculated barriers of transition states is estimated to be ±0.5 kcal mol^{-1} due to errors in accuracy of computations and treatment of hindered rotors and tunneling corrections. The predicted total rate coefficients increase to 2.4−1.1 times the original value in the temperature range 300−3000 K when the calculated barriers of transition states decrease by 0.5 kcal mol^{-1}; they decrease to 0.4−0.9 times when the calculated barriers increase by 0.5 kcal mol^{-1}. The uncertainties are shown as shaded region in Figure 3; they cover the uncertainty range of the experimental data in the whole temperature range.

The branching ratios of channels (1a), (1b), and (1c) predicted with the CVT/SCT method for T = 300−3000 K are plotted in Figure 6. Reaction 1a is the predominant channel for T < 500 K; its branching ratio decreases from 1.00 at 300 K to 0.81 at 1000 K and 0.31 at 3000 K. The branching ratio for reaction 1b is 0.03 at 600 K and increases to 0.15 at 1000 K and 0.49 at 3000 K. The branching ratio for reaction 1c is 0.03 at 1000 K and 0.20 at 3000 K. The branching ratios employed by Marinov are also compared in Figure 6 (dotted lines);[12] branching ratios of k_{1a} appear to be underestimated whereas those of k_{1c} are greatly overestimated throughout the temperature range 300−3000 K.

It should be noted that Marinov reported that reaction 1c is more important than reaction 1b and becomes the most important channel at T > 1400 K, but we predicted reaction 1b to be the most important. On the basis of the PES of channels (1a), (1b), and (1c), the barriers of *trans*- and *gauche*-TS_3 are greater than those of *trans*- and *gauche*-TS_{2a} and TS_{2b}, so it is unlikely that the rate coefficients of reaction 1c are greater than those of reaction 1b, especially at low temperatures. The revised branching ratios for production of CH_3CHOH, CH_2CH_2OH, and CH_3CH_2O should have significant impacts on the chemical modeling of combustion systems involving ethanol, particularly at high temperatures.

Conclusion

Total rate coefficients of the reaction $O(^3P)$ + C_2H_5OH in the temperature range 782−1410 K were determined using a

diaphragmless shock tube with atomic resonance absorption detection of O atoms. Our results extended the upper limit of the temperature range of study from 886 to 1410 K and clearly indicated a non-Arrhenius behavior of the rate coefficient. Rate coefficients obtained in this work is slightly smaller than those determined previously by Grotheer et al.[9] in the overlapped temperature region 782−886 K but within experimental errors. Theoretical calculations at the CCSD(T)/6-311+G(3df, 2p)//B3LYP/6-311+G(3df) level predict transition states and barriers for various channels. Rate coefficients predicted with CVT/SCT show that branching ratios of three accessible reaction channels to form $CH_3CHOH + OH$ (1a), $CH_2CH_2OH + OH$ (1b), and $CH_3CH_2O + OH$ (1c) varies with temperature. At $T < 600$ K, reaction 1a dominates by >96%, whereas, above 2300 K, reaction 1b becomes more important with a branching ratio >44%. The branching for the channel (1c) is less than 12% for $T < 2000$ K. Predicted total rate coefficients are in satisfactory agreement with our experimental data at high temperature (782−1410 K) and those reported previously.

Acknowledgment. Y.-P.L. thanks the National Science Council of Taiwan (Grant No. NSC95-2119-M-009-032) for support. M.C.L. and S.X. thank the support from the Basic Energy Science, Department of Energy, under Contract DE-FG02-97-ER14784, and Cherry L. Emerson Center for Scientific Computation of Emory University for the use of its resources, which are in part supported by a National Science Foundation Grant (CHE-0079627) and an IBM Shared University Research Award. M.C.L. also acknowledges the support from the National Science Council of Taiwan for a Distinguished Visiting Professorship at the National Chiao Tung University in Hsinchu, Taiwan.

References and Notes

(1) Hansen, A. C.; Zhang, Q.; Lyne, P. W. L. *Bioresour. Technol.* **2005**, *96*, 277 and references therein.
(2) Deluga, G. A.; Salge, J. R.; Schmidt, L. D.; Verykios, X. E. *Science* **2004**, *303*, 993.
(3) Kato, A.; Cvetanovic, R. J. *Can. J. Chem.* **1967**, *45*, 1845.
(4) Avramenko, L. I.; Kolesnikova, R. V.; Savinova, G. I. *Bull. Acad. Sci. USSR, Div. Chem. Sci. (Engl. Transl.*) **1967**, *16*, 19.
(5) Avramenko, L. I.; Kolesnikova, R. V. *Bull. Acad. Sci. USSR, Div. Chem. Sci. (Engl. Transl.*) **1971**, *20*, 2700.
(6) Owens, C. M.; Roscoe, J. M. *Can. J. Chem.* **1976**, *54*, 984.
(7) Ayub, A. L.; Roscoe, J. M. *Can. J. Chem.* **1979**, *57*, 1269.
(8) Washida, N. *J. Chem. Phys.* **1981**, *75*, 2715.
(9) Grotheer, H. H.; Nesbitt, F. L.; Klemm, R. B. *J. Phys. Chem.* **1986**, *90*, 2512.
(10) Herron,. J. T. *J. Phys. Chem. Ref. Data* **1988**, *17*, 967.
(11) Held, T. J.; Dryer, F. L. *Int. J. Chem. Kinet.* **1998**, *30*, 805.
(12) Marinov, N. M. *Int. J. Chem. Kinet.* **1999**, *31*, 183.
(13) Dutton, N. J.; Fletcher, I. W.; Whitehead, J. C. *J. Phys. Chem.* **1985**, *89*, 569.
(14) Lu, C.-W.; Chou, S.-L.; Lee, Y.-P.; Xu, S.; Xu, Z. F.; Lin, M. C. *J. Chem. Phys.* **2005**, *122*, 244314.
(15) Koshi, M.; Yoshimura, M.; Fukuda, K.; Matsui, H.; Saito, K.; Watanabe, M.; Imamura, A.; Chen, C. *J. Chem. Phys.* **1990**, *93*, 8703.
(16) Hsiao, C.-C.; Lee, Y.-P.; Wang, N. S.; Wang, J. H.; Lin, M. C. *J. Phys. Chem. A* **2002**, *106*, 10231.
(17) Tsuchiya, K.; Yokoyama, K.; Matsui, H.; Oya, M.; Dupre, G. *J. Phys. Chem.* **1994**, *98*, 8419.
(18) Greene, E. F.; Toennies, J. P. *Chemical Reactions in Shock Waves*; Academic Press: New York, 1964.
(19) Michael, J. V. *J. Chem. Phys.* **1989**, *90*, 189.
(20) Michael, J. V.; Sutherland, J. W. *Int. J. Chem. Kinet.* **1986**, *18*, 409.
(21) Ross, S. K.; Sutherland, J. W.; Kuo, S.-C.; Klemm, R. B. *J. Phys. Chem. A* **1997**, *101*, 1104.
(22) Raghavachari, K.; Trucks, G. J.; Pople, J. A.; Head-Gordon, M. *Chem. Phys. Lett.* **1989**, *157*, 479.
(23) Corchado, J. C.; Chuang, Y.-Y.; Fast, P. L.; Villà, J.; Hu, W.-P.; Liu, Y.-P.; Lynch, G. C.; Nguyen, K. A.; Jackels, C. F.; Melissas, V. S.; Lynch, B. J.; Rossi, I.; Coitiño, E. L.; Fernandez-Ramos, A.; Pu, J.; Albu, T. V.; Steckler, R.; Garrett, B. C.; Isaacson, A. D.; Truhlar, D. G. *POLYRATE* v9.3; 2004.
(24) Frisch, M. J.; Trucks, G. W.; Schlegel, H. B.; Scuseria, G. E.; Robb, M. A.; Cheeseman, J. R.; Zakrzewski, V. G.; Montgomery, J. A., Jr.; Stratmann, R. E.; Burant, J. C.; Dapprich, S.; Millam, J. M.; Daniels, A. D.; Kudin, K. N.; Strain, M. C.; Farkas, O.; Tomasi, J.; Barone, V.; Cossi, M.; Cammi, R.; Mennucci, B.; Pomelli, C.; Adamo, C.; Clifford, S.; Ochterski, J.; Petersson, G. A.; Ayala, P. Y.; Cui, Q.; Morokuma, K.; Malick, D. K.; Rabuck, A. D.; Raghavachari, K.; Foresman, J. B.; Cioslowski, J.; Ortiz, J. V.; Stefanov, B. B.; Liu, G.; Liashenko, A.; Piskorz, P.; Komaromi, I.; Gomperts, R.; Martin, R. L.; Fox, D. J.; Keith, T.; Al-Laham, M. A.; Peng, C. Y.; Nanayakkara, A.; Gonzalez, C.; Challacombe, M.; Gill, P. M. W.; Johnson, B. G.; Chen, W.; Wong, M. W.; Andres, J. L.; Head-Gordon, M.; Replogle, E. S.; Pople, J. A. *Gaussian 03*, revision A.7; Gaussian, Inc.: Pittsburgh, PA, 2003.
(25) Li, J.; Kazakov, A.; Dryer, F. *Int. J. Chem. Kinet.* **2001**, *33*, 859 and references therein.
(26) Yamabe, T.; Koizumi, M.; Yamashits, K.; Tachibana, A. *J. Am. Chem. Soc.* **1984**, *106*, 2255.
(27) Butkovskaya, N. I.; Zhao, Y.; Setser, S. W. *J. Phys. Chem.* **1994**, *98*, 10779.
(28) Park, J.; Zhu, R. S.; Lin, M. C. *J. Chem. Phys.* **2002**, *117*, 3224.
(29) Park, J.; Zhu, R. S.; Lin, M. C. *J. Chem. Phys.* **2003**, *118*, 9990.
(30) Xu, Z. F.; Park, J.; Lin, M. C. *J. Chem. Phys.* **2004**, *120*, 6593.
(31) Feng, R.; Brion, C. E. *Chem. Phys. Lett.* **2002**, *282*, 419.
(32) Cheng, B. M.; Bahou, M.; Chen, W. C.; Yu, C.-h.; Lee, Y.-P.; Lee, L. C. *J. Chem. Phys.* **2002**, *117*, 1633.
(33) FACSIMILE (AEA Technology, Oxfordshire, U.K) is a computer software for modeling process and chemical reaction kinetics.
(34) Li, J.; Kazakov, A.; Dryer, F. L. *J. Phys. Chem. A* **2004**, *108*, 7671.
(35) Ruscic, B.; Boggs, J. E.; Burcat, A.; Csaszar, A. G.; Demaison, J.; Janoschek, R.; Martin, J. M. L.; Morton, M. L.; Rossi, M. J.; Stanton, J. F.; Szalay, P. G.; Westmoreland, P. R.; Zabel, F.; Berces, T. *J. Phys. Chem. Ref. Data* **2005**, *34*, 573.
(36) Ruscic, B.; Berkowitz, J. *J. Chem. Phys.* **1994**, *101*, 10936.
(37) Meier, U.; Grotheer, H. H.; Riekert, G.; Just, T. *Chem. Phys. Lett.* **1985**, *115*, 221.
(38) Mokrushin, W.; Bedanov, V.; Tsang, W.; Zachariah, M.; Knyazev, V. *ChemRate*, version 1.20; National Institute of Standards and Technology: Gaithersburg, MD 20899, 2003.
(39) Tzeng, C. M.; Choi, Y. M.; Huang, C. L.; Ni, C. K.; Lee, Y. T.; Lin, M. C. *J. Phys. Chem. A* **2004**, *108*, 7928.
(40) Srinivasan, N. K.; Su, M.-C.; Sutherland, J. W.; Michael, J. V. *J. Phys. Chem. A* **2005**, *109*, 7902.
(41) Wooldridge, M. S.; Hanson, R. K.; Bowman, C. T. *Int. J. Chem. Kinet.* **1994**, *26*, 389.
(42) Baulch, D. L.; Cobos, C. J.; Cox, R. A.; Esser, C.; Frank, P.; Just, Th.; Kerr, J. A.; Pilling, M. J.; Troe, J.; Walker, R. W.; Warnatz, J. *J. Phys. Chem. Ref. Data* **1992**, *21*, 411.
(43) Tsang, W.; Hampson, R. F. *J. Phys. Chem. Ref. Data* **1986**, *15*, 1087.
(44) Miller, J. A.; Melius, C. F. *Comb. Flame* **1992**, *91*, 21.
(45) Miyoshi, A.; Tsuchiya, K.; Yamauchi, N.; Matsui, H. *J. Phys. Chem.* **1994**, *98*, 11452.
(46) Baulch, D. L.; Cobos, C. J.; Cox, R. A.; Frank, P.; Hayman, G.; Just, Th.; Kerr, J. A.; Murrells, T.; Pilling, M. J.; Troe, J.; Walker, R. W.; Warnatz, J. *J. Phys. Chem. Ref. Data* **1994**, *23*, 847.
(47) Atkinson, R.; Baulch, D. L.; Cox, R. A.; Crowley, J. N.; Hampson, R. F., Jr., Kerr, J. A.; Rossi, M. J.; Troe, J. *J. Phys. Chem. Ref. Data* **1997**, *26*, 521.
(48) Edelbuttel-Einhaus, J.; Hoyermann, K.; Rohde, G.; Seeba, J. *Symp. Int. Combust. Proc.* **1992**, *24*, 661.
(49) Dagaut, P.; Cathonnet, M.; Boettner, J. C. *Int. J. Chem. Kinet.* **1991**, *23*, 437.
(50) Baulch, D. L.; Cobos, C. J.; Cox, R. A.; Frank, P.; Hayman, G.; Just, Th.; Kerr, J. A.; Murrells, T.; Pilling, M. J.; Troe, J.; Walker, R. W.; Wamatz, J. *Comb. Flame* **1994**, *98*, 59.
(51) Lu, C.-W.; Wu, Y.-J.; Lee, Y.-P.; Zhu, R. S.; Lin, M. C. *J. Phys. Chem. A.* **2003**, *107*, 11020.
(52) Grillo, A.; Reed, R.; Slack, M. W. *J. Chem. Phys.* **1979**, *70*, 1634.
(53) Smith, O. I.; Tseregounis, S.; Wang, S.-N. *Int. J. Chem. Kinet.* **1982**, *14*, 679.
(54) Tsang, W. *J. Phys. Chem. Ref. Data* **1980**, *16*, 471.